JGR Space Physics

RESEARCH ARTICLE
10.1029/2022JA031011

Generation of Field-Aligned Currents During Substorm Expansion: An Update

Yusuke Ebihara[1] **and Takashi Tanaka**[2]

[1]Research Institute for Sustainable Humanosphere, Kyoto University, Uji, Japan, [2]International Research Center for Space and Planetary Environmental Science, Kyushu University, Fukuoka, Japan

Key Points:

- We identify the origin of substorm-associated field-aligned current (FAC) by tracing a packet of Alfvén waves in a global MHD simulation
- The FAC is generated in near-earth plasma sheet where azimuthally moving plasma pulls magnetic field lines (near-Earth FAC dynamo)
- The evolution of the substorm is governed by FAC dynamos; flank FAC dynamo for growth phase and near-Earth FAC dynamo for expansion phase

Correspondence to:
Y. Ebihara,
ebihara@rish.kyoto-u.ac.jp

Citation:
Ebihara, Y., & Tanaka, T. (2023). Generation of field-aligned currents during substorm expansion: An update. *Journal of Geophysical Research: Space Physics*, *128*, e2022JA031011. https://doi.org/10.1029/2022JA031011

Received 13 SEP 2022
Accepted 16 JAN 2023

Author Contributions:
Conceptualization: Yusuke Ebihara
Data curation: Yusuke Ebihara
Formal analysis: Yusuke Ebihara
Funding acquisition: Yusuke Ebihara
Investigation: Yusuke Ebihara
Methodology: Yusuke Ebihara
Resources: Yusuke Ebihara
Software: Yusuke Ebihara, Takashi Tanaka
Validation: Yusuke Ebihara
Visualization: Yusuke Ebihara
Writing – original draft: Yusuke Ebihara
Writing – review & editing: Yusuke Ebihara, Takashi Tanaka

Abstract We investigated generation processes of field-aligned currents (FACs) that are abruptly intensified at the beginning of the substorm expansion phase by tracing a packet of the Alfvén wave backward in time from the onset position in the ionosphere in the global magnetohydrodynamics (MHD) simulation. The generation region is found in the near-Earth plasma sheet, in which (a) azimuthally moving plasma pulls the magnetic field line, and performs negative work against the magnetic tension force to excite the Alfvén waves, (b) FACs are generated from the requirement of Ampère and Faraday laws, and (c) field-perpendicular current is converted to FACs. We call this near-Earth FAC dynamo. The plasma involved originates in the tail lobe region. When near-Earth reconnection occurs in the plasma sheet, the plasma is accelerated earthward by the Lorentz force, and decelerated by the plasma pressure gradient force, followed by the Lorentz force. The flow is deflected to the west and east directions by the plasma pressure gradient force and the Lorentz force, resulting in the excitation of Alfvén waves and FACs. The Alfvén waves propagate along the magnetic field in the rest frame of the moving plasma. When it arrives at the ionosphere, the auroral electrojet starts developing and the substorm expansion phase begins. The near-Earth FAC dynamo can be distinguished from the near-Earth dynamo ($\mathbf{J} \cdot \mathbf{E} < 0$, where $\mathbf{J}$ is the current density and $\mathbf{E}$ is the electric field). We suggest that the evolution of the substorm can be understood in terms of the development of FACs.

Plain Language Summary Abrupt intensification of field-aligned currents (FACs) is one of the manifestations of substorms, which result in bright aurora and auroral electrojet. The FACs are also important to supply energy to the polar ionosphere, in which a large amount of energy ($\sim 10^{11}$ W) is consumed during the substorms. The origin of the substorm-associated FAC is a long-lasting issue, and not well understood. To identify the processes involved in the generation of the substorm-associated FACs, we performed global magnetohydrodynamics (MHD) simulation, and traced a packet that is supposed to carry the perturbations associated with the FACs. With this new method, we found that the substorm-associated FACs are generated in the near-Earth region near midnight where the plasma pulls the magnetic field lines to excite the Alfvén waves carrying FACs. A series of processes from the near-Earth reconnection to the sudden intensification of the auroral electrojet (auroral breakup) becomes clearer than ever.

1. Introduction

Substorm expansion onset is manifested by sudden brightening of aurora (Akasofu, 1964) and sudden development of auroral electrojet flowing in the east-west direction (Kamide & Brekke, 1975). At the same time, the field-aligned currents (FACs) are enhanced, which are thought to be closely related to the bright aurora and the intensification of the auroral electrojet (Connors et al., 2014; Cummings et al., 1968; Gjerloev & Hoffman, 2014; Hughes & Rostoker, 1979; Kamide & Akasofu, 1976; Kamide et al., 1989; Murphy et al., 2013; Rostoker et al., 1975). Boström (1964) suggested two types of FACs associated with substorms, Type 1 and Type 2. Type 1 current, flowing into the ionosphere on the dawnside and away on the duskside, is supposed to be connected to the partial ring current and/or the cross-tail current (Crooker & McPherron, 1972; Kamide et al., 1976; Kamide & Fukushima, 1972; Mcpherron et al., 1973; Meng & Akasofu, 1969). Boström's Type 2 current consists of downward current in the poleward region, and upward current in the equatorward region. Using data from the Triad satellite, Iijima and Potemra (1976) showed two pairs of FACs encircling the geomagnetic pole. One is called Region 1 current, which flows in the poleward part, and the other one is called Region 2 current, which flows in the equatorward part. The Region 1 current flows into the ionosphere on the dawnside, and away from it on the duskside. The polarity of the Region 2 current is opposite to that of the Region 1 current. When the substorm activity increases, the latitudinal width of the Region 1 and 2 currents increase by factors of 1.2–1.3,

and the center of the regions shift equatorward on average (Iijima & Potemra, 1978). Active Magnetosphere and Planetary Electrodynamics Response Experiment (AMPERE) can capture snapshots of the FACs at high-cadence (∼10 min) with the Iridium constellation that comprises 66 satellites (Anderson et al., 2014). During the substorm expansion, the net FAC is shown to increase by $\sim 10^6$ A and the Region 1-sence FAC is more intensified than the Region 2-sense FAC (Coxon et al., 2014b). The Region 1-sence and Region 2-sence FACs are intensified on the nightside at 64–75 magnetic latitudes (MLATs) for the substorm onsets taking place at 64–68 MLAT (Coxon et al., 2017).

The generation of the substorm-associated FACs is problematic, and a long-lasting issue. Observations have shown that the substorm-associated FACs are associated with the earthward fast flow of plasma in the near-Earth tail region (Angelopoulos et al., 1996; Fairfield et al., 1998; Hones, 1979). The earthward flow is observed to divert eastward and westward (Nagai et al., 2000). The diversion of the flow results in accumulation of positive and negative space charge on the dawnside and duskside, respectively, which is in favor of the generation of Region 1-sense FACs (Birn and Hesse, 1991, 1996; Keiling et al., 2009; Nakamura et al., 1993). The earthward flow is likely triggered by the near-Earth reconnection that is known to occur just prior to the onset of the expansion (Angelopoulos et al., 2008; Baker et al., 2002; Hones et al., 1973; Ieda et al., 2008; Machida et al., 2009; Miyashita et al., 2009; Nishida & Nagayama, 1973; Runov et al., 2008; Sergeev et al., 1995; Yao et al., 2012). The FAC is suggested to be generated far from the reconnection site (Keiling et al., 2009), or near the reconnection site (Baker et al., 1993). Nagai and Shinohara (2021) suggested that the upward FACs are generated both far from and near the reconnection site. Numerical simulations have supported the ideas that the FACs are generated far from the reconnection site due to flow shear (Birn and Hesse, 1991, 1996, 2013; Ebihara & Tanaka, 2015a, 2015b; Hesse & Birn, 1991; Tanaka, 2015; Tanaka et al., 2017, 2021), and near the reconnection site (Pritchett & Coroniti, 2004; Shay et al., 2011; Zenitani & Nagai, 2016). The ground based observation shows that the expansion onset usually takes place in the most equatorward auroral arcs (Akasofu, 1964), which may favor the near-Earth region, rather than the reconnection site for the initiation of the expansion onset (Lui, 1996, 2015).

The earthward flow is decelerated in the near-Earth plasma sheet (Shiokawa et al., 1997). The braking of the earthward flow results in the inertial current flowing in the eastward direction, which forms the Region 1-sense FACs (Haerendel, 1992; Shiokawa et al., 1997). The total inertial current is estimated to be 7×10^4 A on the basis of observation (Shiokawa et al., 1997) and 3×10^5 A on the basis of simulation (Birn et al., 1999). The overall increase in the FACs during the substorm expansion is $\sim 10^6$ A (Coxon et al., 2014a; Kamide & Baumjohann, 1985), which is larger than the total inertial current. Shiokawa et al. (1998) suggested that the substorm-associated FACs result from the diversion of the current associated with the pressure gradient, rather than the inertial current. Intrusion of low-entropy plasma in the plasma sheet, known as a bubble, is also proposed to form the FACs due to current continuity (Chen & Wolf, 1993; Yang et al., 2012), and to trigger the expansion onset (Lyons et al., 2010; Nishimura et al., 2010).

Large-amplitude oscillations of the magnetic field are observed in the near-Earth plasma sheet at the expansion onset (Takahashi et al., 1987). It is also assumed that the frozen-in condition is broken, and the cross-tail current is collapsed (Lui, 1991, 2011) due to ballooning instability (Cheng & Lui, 1998; Pu et al., 1992; Roux et al., 1991; Xing et al., 2013) and cross-field current instability (Lui et al., 1991). The collapse of the cross-tail current results in the formation of the substorm-associated FACs to conserve the current continuity (Lui, 1996). Lui (1996) estimated the upward FAC in the ionosphere, which is comparable to the observed values. Auroral bead structures are known to appear along the pre-existing arc at the auroral breakup (Donovan et al., 2006; Motoba et al., 2012; Sakaguchi et al., 2009). Similar bead structures were observed in the conjugates points in the Northern and Southern Hemispheres, suggesting that the origin is most likely located in the magnetosphere (Motoba et al., 2012). The auroral bead structures are thought to be the ionospheric manifestation of the current disruption (Donovan et al., 2006), and the ballooning-interchange instability (Sorathia et al., 2020).

The magnitude of the FACs in the ionosphere has been quite often evaluated by integrating the divergence of the perpendicular current along a magnetic field line (Hasegawa & Sato, 1979; Sato & Iijima, 1979; Vasyliunas, 1984). The perpendicular current can be determined from the momentum equation that includes the term related to the Lorentz force. The evaluation of the FAC is challenging because of the limited number of data points. Flow shear observed in the plasma sheet is often used to evaluate the FACs in the ionosphere with the assumption that the FAC is generated in a vertically limited region (Keiling et al., 2009; Lui, 1996; Shiokawa et al., 1998), or along

the entire field line (Birn & Hesse, 2013; Vasyliunas, 1970; Yang et al., 2012; Yao et al., 2012). A few concerns arise in the use of the field-line integral of the perpendicular current for the evaluation of FACs. First, there is no guarantee that the perpendicular current is distributed in the same way along the magnetic field line. Ebihara and Tanaka (2015b) showed the simulation results that the perpendicular current varies considerably over the magnetic field line during the expansion phase of a substorm. Secondly, the Alfvén waves will divert the original magnetic field line if the speed of ambient plasma is nonnegligible in comparison with the Alfvén speed (Mallinckrodt & Carlson, 1978; Maltsev et al., 1977; Neubauer, 1980; Wright & Southwood, 1987). If the FAC is carried by Alfvén wave, the FAC does not always propagate along the magnetic field line. In that case, the FAC is no longer "field-aligned" in the quasi-inertial frame of reference. During the substorm expansion, the convective motion of plasma is high (Angelopoulos et al., 2008; Baker et al., 2002; Hones et al., 1973; Ieda et al., 2008; Machida et al., 2009; Miyashita et al., 2009; Nishida & Nagayama, 1973; Runov et al., 2008; Sergeev et al., 1995; Yao et al., 2012) whereas the Alfvén speed is relatively slow in the plasma sheet (Mallinckrodt & Carlson, 1978). Thus, it is not straightforward to assume that the FACs propagate along the magnetic field line. The last concern is the travel time of the Alfvén waves. The substorm expansion is a transient phenomenon, so that time-dependent variations of the perpendicular current may be significant.

Energy is also a matter to be solved. During the substorm expansion, a large amount of energy is consumed in the ionosphere as Joule dissipation. Observations have shown that the Joule dissipation rate is estimated to $\sim 10^{11}$ W during the substorm expansion (Ahn et al., 1983; Kamide et al., 1986; Palmroth et al., 2005; Richmond et al., 1990; Sun et al., 1985). Since the ionosphere is a load, a dynamo (generator) must exist in the magnetosphere to supply the magnetic energy into the polar ionosphere, most likely, by the Alfvén waves. Because of the low-frequency limit, the electric energy can be neglected. Many studies have been made to search for the dynamo region where $\mathbf{J} \cdot \mathbf{E} < 0$, where $\mathbf{J}$ is the current density (Akasofu, 2013; Birn & Hesse, 2005; Ebihara & Tanaka, 2015a, 2015b; Hamrin et al., 2006; Lui, 1996; Marghitu et al., 2006; Rostoker & Boström, 1976; Tanaka et al., 2010, 2017). Lui and Kamide (2003) pointed out that electrons are well magnetized whereas ions are unmagnetized in the plasma sheet during the substorm expansion. The electrons moving earthward generate anti-sunward electric field, which acts as dynamo of Boström's Type 2 current (Boström, 1964). Direct observations of $\mathbf{J}\cdot\mathbf{E}$ in the plasma sheet were conducted by Hamrin et al. (2011) who demonstrated that the dynamo region (where $\mathbf{J}\cdot\mathbf{E} < 0$) appears in close conjunction with the high-speed flow of plasma. Global MHD simulations show that the dynamo region (where $\mathbf{J}\cdot\mathbf{E} < 0$) appears in the near-Earth region in conjunction with the appearance of the FACs (Birn & Hesse, 2005; Ebihara & Tanaka, 2015a, 2015b; Tanaka, 2015). It has been thought that the FACs are generated in the region where $\mathbf{J}\cdot\mathbf{E} < 0$ (Cravens, 1997), but this idea may not be straightforwardly applied for general situations. As explained below, $\mathbf{J}\cdot\mathbf{E}$ consists of two terms in the MHD approximation. One is associated with the magnetic tension force, and the other one is associated with the magnetic pressure force. The generation of FAC, namely the excitation of Alfvén waves, is related to the former one because of the nature of the Alfvén waves. Thus, the negative $\mathbf{J}\cdot\mathbf{E}$ does not always mean the generation of the Alfvén waves.

Most of the previous studies have taken into consideration the current continuity of the current along the magnetic field line, or the polarity of $\mathbf{J}\cdot\mathbf{E}$ for the study on the generation of the FACs associated with substorms. However, there are some concerns about the methodology as mentioned above. The purpose of this study is to clarify the generation mechanism of the substorm-associated FACs by employing the new method recently introduced by Ebihara and Tanaka (2022). Ebihara and Tanaka (2022) traced a packet that is supposed to carry the disturbances associated with the Alfvén wave. The Region 1 FACs were found to be generated in the flank magnetopause where the solar wind-originated plasma pulls the newly reconnected magnetic field lines. The generation region is far from the original magnetic field line extending from the ionosphere because of the fast plasma flow in comparison with the Alfvén speed. In this study, we also traced the packet of the Alfvén wave backward in time from the onset position in the ionosphere. We searched for the generation region and the generation processes of the substorm-associated FAC by focusing on the following three aspects that are based on fundamental physics. (a) *Continuity of the current*. When the FACs are generated, the divergence of the FACs is nonzero. However, the divergence of the FACs does not tell us the reason why the FACs are generated. (b) *Rate of change in the FAC in accordance with Ampère and Faraday laws*. The rate of change in the FAC will be nonzero where the FACs are generated. However, the rate can also be nonzero outside the generation region where the Alfvén waves propagate. Thus, the use of the rate is insufficient to identify the generation region. (c) *Negative work of plasma against the magnetic tension force*, which is supposed to result in excitation of the Alfvén waves. Note that the generation of the Alfvén waves does not always mean the generation of FACs (Cravens, 1997). Thus, we considered all the three aspects to specify the possible generation region and mechanism of the FACs associated with substorms.

2. Simulation

We used the global MHD simulation (REPPU) developed by Tanaka (2015). The grid system and the parameters are exactly the same as those used by Ebihara and Tanaka (2015b). The following is a brief description for the MHD simulation and parameters. The MHD equations were solved in the magnetospheric domain that ranges from the geocentric distance of 2.6 R_E to 200 R_E at midnight and 600 R_E at noon. The inner boundary of the magnetospheric domain (2.6 R_E) is connected to the ionosphere by the dipole magnetic field. In the ionospheric domain, an elliptic partial differential equation was solved to obtain the electric potential for given FACs and ionospheric conductivity. The ionospheric conductivity was assumed to increase in accordance with the following three sources, (a) solar EUV, (b) precipitation of electrons associated with diffuse aurora, and (c) precipitation of electrons associated with discrete aurora. For (a), the ionospheric conductivity is determined by the solar zenith angle. For (b), the ionospheric conductivity was calculated on the basis of the FACs, the plasma pressure and the temperature mapped from the inner boundary of the magnetospheric domain to the ionosphere along the dipole magnetic field. For (c), the conductivity increases in accordance with the magnitude of the upward FAC. We mapped the calculated electric field from the ionosphere to the inner boundary of the magnetospheric domain along the dipole magnetic field. Readers may refer Ebihara et al. (2014) who explained the calculation of the conductivity in detail.

The origin of the coordinate is located at the center of the Earth. x and y point toward the Sun and dusk, respectively. z is antiparallel to the Earth's dipole moment. First, we imposed the steady solar wind condition for 2 hr with solar wind velocity of (−372, 0, 0) km/s, solar wind density of 5 cm^{-3}, IMF of (0, 2.5, 5.0) nT. At t = 120 min, we changed the z-component of IMF B_z to −5.0 nT, and increased the x-component of the solar wind velocity V_x to 500 km/s. All the solar wind parameters were held constant after t = 120 min. After the southward turning of IMF, the auroral electrojet starts developing gradually, which can be regarded as the growth phase of a substorm. At t ∼177 min, the field-aligned current and the westward auroral electrojet abruptly increased in the ionosphere, which corresponds to the beginning of the expansion phase of the substorm.

3. Basic Equations and Methodology

3.1. Current Continuity

From the requirement of the current continuity ($\nabla\cdot\mathbf{J} = 0$, where $\mathbf{J}$ is the current density), the following equation must be satisfied as

$$\nabla \cdot \mathbf{J}_{\parallel} = -\nabla \cdot \mathbf{J}_{\perp}. \tag{1}$$

The subscripts ∥ and ⊥ indicate the quantities parallel and perpendicular to the magnetic field, respectively. The field-perpendicular current $\mathbf{J}_\perp$ is given by the momentum equation as

$$\begin{aligned}\mathbf{J}_{\perp} &= \frac{\mathbf{B}\times\nabla P}{B^2} + \frac{\mathbf{B}}{B^2}\times\left(\rho\frac{d\mathbf{V}_{\perp}}{dt}\right)\\ &\equiv \mathbf{J}_d + \mathbf{J}_i,\end{aligned} \tag{2}$$

where

$$\mathbf{J}_d = \frac{\mathbf{B}\times\nabla P}{B^2}, \tag{3}$$

$$\mathbf{J}_i = \frac{\mathbf{B}}{B^2}\times\left(\rho\frac{d\mathbf{V}_{\perp}}{dt}\right), \tag{4}$$

and P is the plasma pressure. $\mathbf{J}_d$ and $\mathbf{J}_i$ are called the diamagnetic current, and the inertial current, respectively. Equation (1) describes the conversion between the field-perpendicular currents and FACs, but does not tell us the reason why the FACs are generated.

3.2. Rate of Change in Field-Aligned Currents

From Faraday's and Ampère laws, the rate of change in the FAC $J_\parallel$ is given by (Song & Lysak, 2001a, 2001b)

$$\frac{\partial J_{\parallel}}{\partial t} = -\frac{1}{\mu_0}[\nabla \times \nabla \times \mathbf{E}]_{\parallel}. \tag{5}$$

The right-hand side of Equation (5) consists of two terms (Itonaga et al., 2000) as

$$\frac{\partial J_{\parallel}}{\partial t} = -\frac{\nabla_{\parallel}(\nabla \cdot \mathbf{E})}{\mu_0} + \frac{\left(\nabla^2 \mathbf{E}\right)_{\parallel}}{\mu_0}. \tag{6}$$

The first term on the right-hand side of Equation (6) implies that the field-aligned current is generated when the field-aligned gradient of space charge $\nabla \cdot \mathbf{E}$ is present. Note that in the ideal MHD approximation (in which the resistivity is zero), $E_{\parallel}$ is absent, and only $\mathbf{E}_{\perp}$ is present. However, the second term arises when the magnetic field line is curved. As mentioned below, both the terms are likely important and nonnegligible in the generation region. We calculated these terms as

$$\frac{\nabla_{\parallel}(\nabla \cdot \mathbf{E})}{\mu_0} = \frac{\nabla(\nabla \cdot \mathbf{E})}{\mu_0} \cdot \frac{\mathbf{B}}{B}$$

and

$$\frac{\left(\nabla^2 \mathbf{E}\right)_{\parallel}}{\mu_0} = \frac{\left(\nabla^2 \mathbf{E}\right)}{\mu_0} \cdot \frac{\mathbf{B}}{B}$$

respectively. We calculated $\nabla^2 \mathbf{E}$ by the fourth order finite difference method.

3.3. Generation of Alfvén Wave

If FACs are carried by the Alfvén waves (Kivelson, 2004), the magnetic energy will be transported parallel and antiparallel to the magnetic field. Thus, magnetic energy must be supplied to excite the Alfvén waves. According to Poynting's theorem, the magnetic energy increases when $\mathbf{J} \cdot \mathbf{E} < 0$. Here, the electric energy is neglected because of the low frequency limit. With Ohm's law ($\mathbf{E} = -\mathbf{V} \times \mathbf{B}$), $\mathbf{J} \cdot \mathbf{E}$ can be rewritten as

$$\begin{aligned} \mathbf{J} \cdot \mathbf{E} &= \mathbf{V} \cdot (\mathbf{J} \times \mathbf{B}) \\ &= \mathbf{V} \cdot \left(\frac{\nabla \times \mathbf{B}}{\mu_0} \times \mathbf{B} \right) \\ &= \mathbf{V} \cdot \left[\frac{B^2}{\mu_0} (\mathbf{b} \cdot \nabla)\mathbf{b} - \nabla_{\perp} \left(\frac{B^2}{2\mu_0} \right) \right] \\ &\equiv \mathbf{V} \cdot (\mathbf{F}_t + \mathbf{F}_m), \end{aligned} \tag{7}$$

where $\mathbf{b}$ is the unit vector of the magnetic field ($=\mathbf{B}/B$). $\mathbf{F}_t$ and $\mathbf{F}_m$ are the magnetic tension force and the magnetic pressure force, respectively as

$$\begin{aligned} \mathbf{F}_t &\equiv \frac{B^2}{\mu_0} (\mathbf{b} \cdot \nabla)\mathbf{b}, \\ \mathbf{F}_b &\equiv -\nabla_{\perp} \left(\frac{B^2}{2\mu_0} \right). \end{aligned} \tag{8}$$

To excite the Alfvén waves, magnetic tension must be created. In other words, plasma must perform negative work against the magnetic tension force, that is, $\mathbf{V} \cdot \mathbf{F}_t < 0$. Note that the generation of the Alfvén wave does not always mean the generation of the FACs (Cravens, 1997). To specify the generation region more correctly, we searched for the region that satisfies the three aspects, that is, the current continuity, the rate of change in the FACs, and excitation of the Alfvén waves.

3.4. Packet of Alfvén Wave

The group velocity of the Alfvén wave is parallel or antiparallel to the background magnetic field in the rest frame of the moving medium (Walker, 2008). We assume that the perturbation associated with the FACs propagates at the characteristic velocity $\mathbf{v}$ (Neubauer, 1980; Wright & Southwood, 1987) as

$$\mathbf{v}^{\pm} = \pm\mathbf{V}_A + \mathbf{V}, \tag{9}$$

where $\mathbf{V}_A$ is the Alfvén velocity($=\mathbf{B}/(\mu_0\rho)^{1/2}$, and ρ is the mass density of plasma. We introduced a packet carrying the perturbation associated with the FACs (Ebihara & Tanaka, 2022). The position vector of the packet can be obtained by

$$\mathbf{r}^{\pm}(t) = \int_0^t \mathbf{v}^{\pm}(\mathbf{r}, \tau)d\tau + \mathbf{r}_0, \tag{10}$$

where $\mathbf{r}_0$ is the initial position.

3.5. Energy Conversion Rate

We also considered the energy conversion rates for the 3 types of energy, the magnetic energy, the kinetic energy, and the internal energy (Birn & Hesse, 2005). According to Poynting's theorem, the conservation equation for the magnetic energy is given by

$$\frac{\partial}{\partial t}\left(\frac{B^2}{2\mu_0}\right) + \nabla\cdot\mathbf{S} = -\mathbf{J}\cdot\mathbf{E} = -\mathbf{V}\cdot(\mathbf{J}\times\mathbf{B}), \tag{11}$$

where $\mathbf{S}$ is the Poynting flux ($=\mathbf{E}\times\mathbf{B}/\mu_0$). The right-hand side of Equation (11) governs the conversion of energy. When $\mathbf{J}\cdot\mathbf{E}$ is negative, the magnetic energy increases. Here, we omitted the electric energy. Note that $\mathbf{J}\cdot\mathbf{E}$ can be divided into two terms as indicated by Equation (7), that is, $\mathbf{V}\cdot\mathbf{F}_t$ and $\mathbf{V}\cdot\mathbf{F}_m$. The conservation equation for the kinetic energy is given by

$$\frac{\partial}{\partial t}\left(\frac{\rho}{2}V^2\right) + \nabla\cdot\left(\frac{\rho}{2}V^2\mathbf{V}\right) = \mathbf{V}\cdot(\mathbf{J}\times\mathbf{B} - \nabla P), \tag{12}$$

where ρ is the mass density of plasma. The kinetic energy increases when $\mathbf{V}\cdot(\mathbf{J}\times\mathbf{B}-\nabla P)$ is positive. The conservation equation for the internal energy is given by

$$\frac{\partial u}{\partial t} + \nabla\cdot(\gamma u\mathbf{V}) = \mathbf{V}\cdot\nabla P, \tag{13}$$

where u is the internal energy density of plasma ($=3P/2$), and γ is the ratio of specific heat ($=5/3$). The internal energy increases when $\mathbf{V}\cdot\nabla P$ is positive.

4. Results

Figure 1 summarizes the simulated auroral electrojet (*AE*) indices and the FACs obtained at the ionosphere in the Northern Hemisphere. The auroral electrojet indices were calculated from the ground magnetic disturbances induced by the ionospheric Hall current at magnetic latitudes (MLATs) ranging from 50° to 90° with a regular interval of 1° and 0.5 hr in magnetic local time (MLT). The concept is the same as that for the SuperMAG electrojet index in which a large number of geomagnetic variations (typically more than 100) are used to capture the overall variation of the auroral electrojet (Newell & Gjerloev, 2011). Hereinafter, we refer it as *AE* (1920), or simply *AE*. The numerical figure of 1920 comes from the number of points to be considered in the calculation. Following the original concept of *AE* (Davis & Sugiura, 1966), we call the upper and lower envelopes of the superposed magnetic disturbances *AU* and *AL*, respectively. When the southward IMF arrives at the magnetosphere, the magnitudes of *AU* and *AL* start increasing at $t \sim 122$ min, resulting from the increase in the ionospheric Hall current. After a while, *AL* starts decreasing rapidly at $t \sim 177$ min. We call this moment the onset of the substorm expansion.

The spatial distributions of the FACs at $t = 175.0$–180.0 min are also shown in Figure 1. At a glance, two pairs of the large-scale FACs are clearly demonstrated. For the poleward pair, the current flows into the ionosphere on the dawnside and away from the ionosphere on the duskside. For the equatorward pair, the polarities of the currents are almost opposite. They resemble Region 1 and Region 2 currents (Iijima & Potemra, 1976; Zmuda & Armstrong, 1974). At $t = 178$ min (~1 min after the onset determined by the sudden decrease in *AL*), the

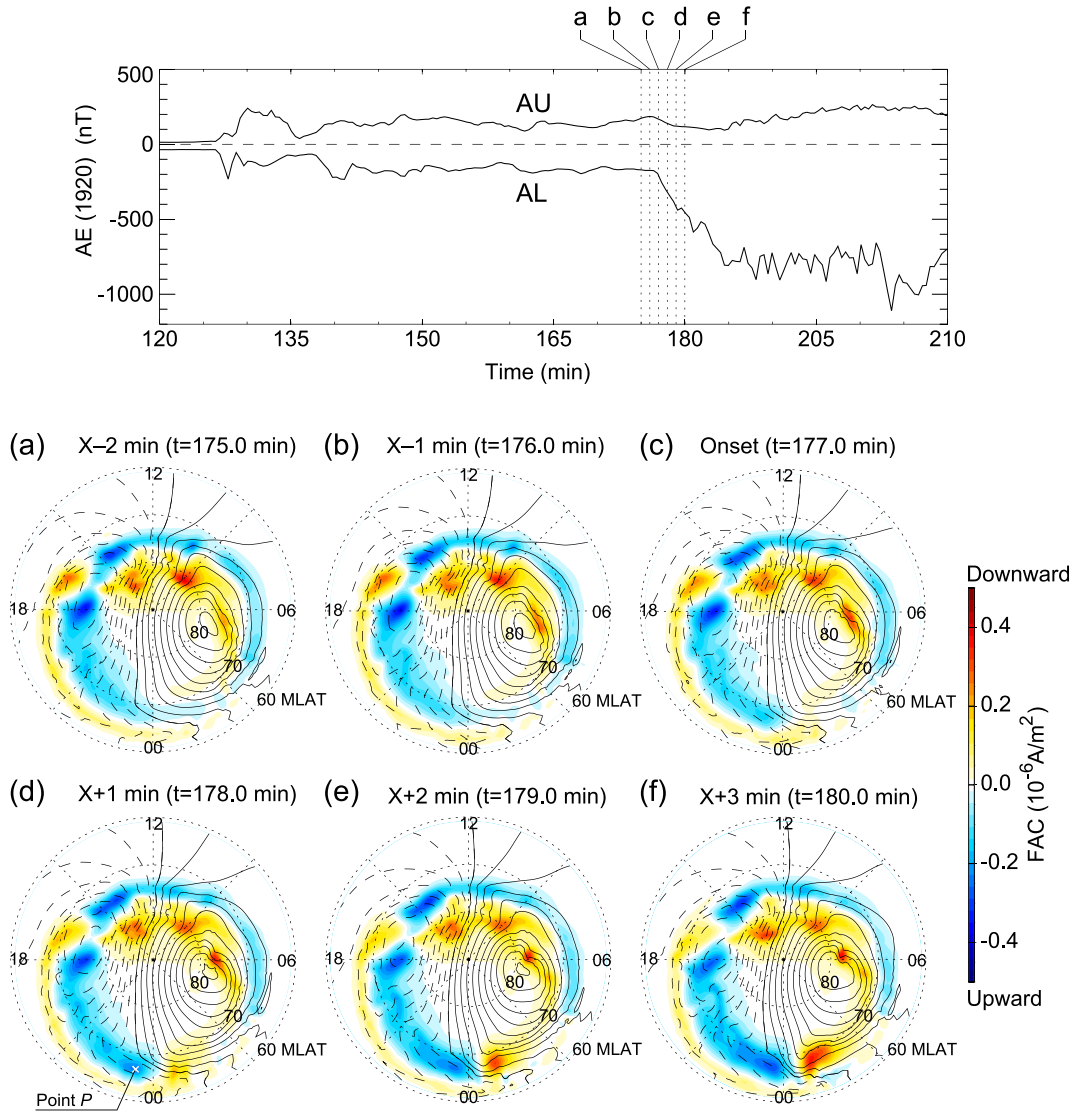

Figure 1. (top) Simulated auroral electrojet indices *AE* (1920), and (bottom) field-aligned currents at the ionospheric altitude in the Northern Hemisphere at $t = 175.0$ min (2 min before the onset), 176.0 min (1 min before the onset), 177.0 min (onset), 178.0 min (1 min after the onset), 179 (2 min after the onset), and 180 min (3 min before the onset). Positive (negative) values indicate downward (upward) field-aligned currents. Sun is to the top, and the outermost circle represents the magnetic latitude (MLAT) of 60°. The contour lines indicate equipotential lines with an interval of 5 kV. The solid (dashed) contour lines represent positive (negative) potential, respectively, and that the generation regions are not clearly identified. The whitish "×" symbol (66.6 MLAT and 23.4 MLT) represents the position where the magnitude of the upward field-aligned current is maximized at $t = 178$ min around midnight.

enhancement of the upward FAC becomes clear in the premidnight region. At this moment, the magnitude of the upward FAC is maximized at 66.6 MLAT and 23.4 MLT, which is marked by the white "×" symbol. Hereinafter, we call this point *P*. After that, the upward FAC increases with time and the large-amplitude upward FAC expands westward and poleward.

Figure 2 is a perspective view of the magnetosphere. The short cylinders indicate the positions of the packet that reaches the point *P* at $t = 178.0$ min. First, we traced the packet from the point *P* in the ionosphere to the spherical surface at geocentric distance of 3.8 R_E along the dipole magnetic field line. We call this point *P*'. That is because the MHD equations were not solved at < 2.6 R_E, and the number density of plasma near the inner boundary (~2.6 R_E) suffers from some unwanted perturbations arising from numerical issues. To avoid uncertainty in the calculation of the Alfvén velocity, we skipped this region. We chose $\mathbf{v}^+$ that travels toward the ionosphere in the Northern

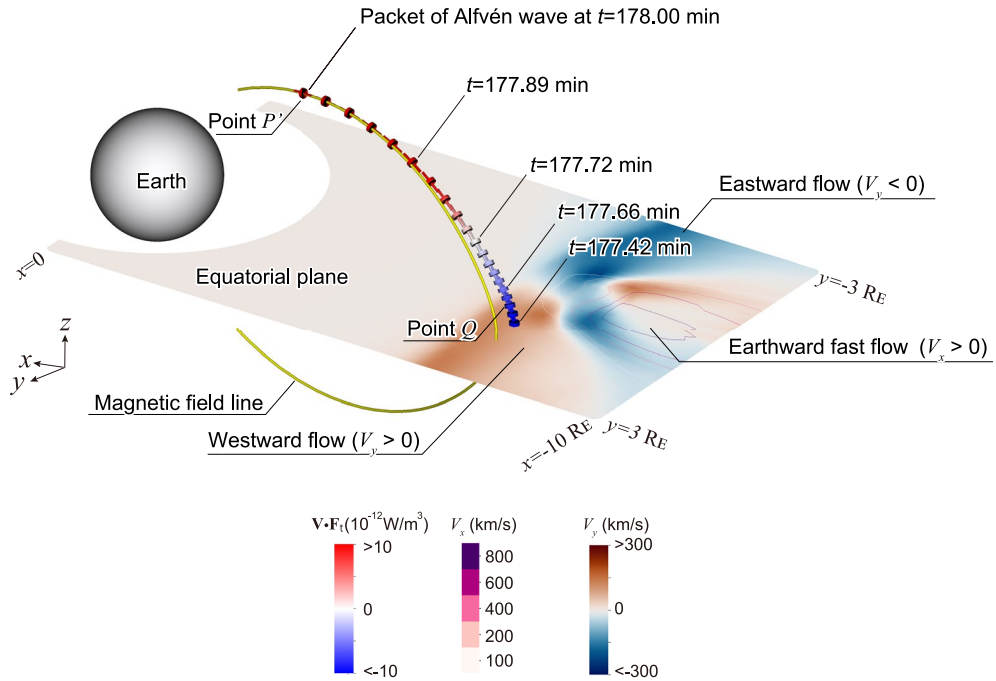

Figure 2. A perspective view of the magnetosphere from the nightside. The small cylinders indicate the positions of the packet from 177.42 min (equatorial plane) to 178.00 min, which are supposed to carry perturbations associated with the FACs at the point P at $t = 178.0$ min. Color on the magnetic field line indicates the value of $\mathbf{V}\cdot\mathbf{F}_t$, where $\mathbf{V}$ is the plasma velocity and $\mathbf{F}_t$ is the magnetic tension force. The thin tubes extending from the cylinders indicate the magnetic field lines. The horizontal plane represents the equatorial plane (from $x = -10$ R_E to 0, and $y = -3$ to 3 R_E.) Color shaded on the equatorial plane represents the y-component of plasma velocity (V_y). Color of the contour lines indicates the x-component of plasma velocity (V_x). The simulation result obtained at $t = 177.79$ min are used to draw $\mathbf{F}_t$, the magnetic field line (line integral of $\mathbf{B}$). The points P' and Q are also shown.

Hemisphere, and traced the packet backward in time from P' by using the velocity determined by Equation (9). The packet is found to pass through the equatorial plane at $t = 177.42$ min. Near the equatorial plane, the packet is located in the region where the plasma flows westwardly ($V_y > 0$). The region is westside of the earthward fast flow ($V_x > 0$) triggered by near-Earth reconnection. As explained below, the earthward fast flow is diverted to the dawn and dusk directions. The color code on the cylinders indicates the value of $\mathbf{V}\cdot\mathbf{F}_t$. $\mathbf{V}\cdot\mathbf{F}_t$ is obviously negative near the equatorial plane, indicating that the Alfvén waves are supposed to be excited there.

Figure 3 is also a perspective view of the magnetosphere looking toward the center of the Earth at the equatorial plane at 23.5 MLT. Two magnetic field lines are drawn from selected positions of the packet. The magnetic field lines are bent near the equatorial plane. That is, the magnetic tension force is eastward (toward midnight). The bent field line has been pointed out by Birn and Hesse (1996) to demonstrate the presence of the magnetic shear. The plasma moves westward, so that the plasma performs negative work against the magnetic tension force, that is, $\mathbf{V}\cdot\mathbf{F}_t$, <0. In other words, the kinetic energy of plasma is converted to the magnetic energy. The converted magnetic energy will be transported to the ionosphere by the Alfvén waves.

Figure 4 summarizes relevant quantities taken along the trajectory of the packet arriving at the point P at $t = 178.00$ min (~1 min after the onset). They are plotted as a function of arc length (distance) D from the point P' (whose footprint is P, i.e., 66.6 MLAT and 23.4 MLT) along the trajectory. As shown in Figures 4a and 4b, the packet crossed the equatorial plane ($z = 0$) at $t \sim 177.4$ min, and moved into the Northern Hemisphere from the Southern Hemisphere. Here, we focus on the quantities taken in the Northern Hemisphere because FAC is zero near the equatorial plane, and the FAC at the point P is supposed to be generated in the Northern Hemisphere. Figure 4c shows the normalized FAC (negative upward), $(B_i/B)J_\parallel$, where B_i is the magnetic field at the ionosphere. For the sake of simplicity, B_i is assumed to be 50,000 nT. The choice of B_i does not affect the conclusion. The magnitude of the normalized FAC is zero near the equatorial plane. However, it increases with decreasing D (as the packet proceeds toward the Earth), and maximized at $D \sim 3.0$–4.5 R_E. Figure 4d shows $\nabla\cdot\mathbf{J}_\parallel$, $\nabla\cdot\mathbf{J}_d$, and $\nabla\cdot\mathbf{J}_i$.

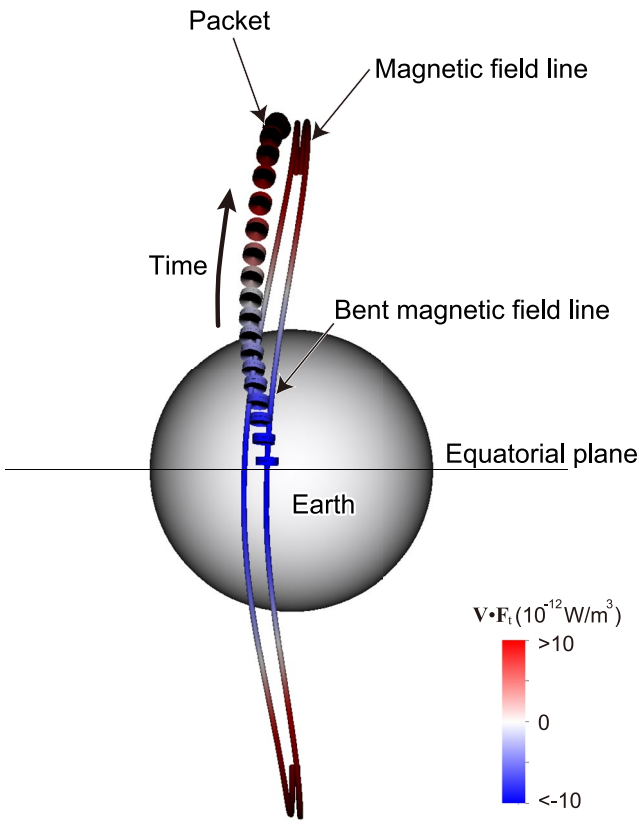

Figure 3. A perspective view of the magnetosphere from 23.5 MLT in the equatorial plane. The small cylinders indicate the positions of the packet that is supposed to carry perturbations associated with the FACs at the point P at $t = 178.0$ min. The thin tubes indicate the magnetic field lines extending from the packets. Color code indicates the value of $\mathbf{V}\cdot\mathbf{F}_t$. The magnetic field lines are bent near the equatorial plane. The magnetic tension force is eastward, whereas the plasma moves westward. Hence, $\mathbf{V}\cdot\mathbf{F}_t < 0$ near the equatorial plane. The simulation result obtained at $t = 177.94$ min are used to draw $\mathbf{F}_t$ and the magnetic field line (line integral of $\mathbf{B}$).

$\mathbf{J}_d$ and $\mathbf{J}_i$ are the diamagnetic currents and the inertial currents, and given by Equations (3) and (4), respectively. Near the equatorial plane, $\nabla\cdot\mathbf{J}_{\parallel}$ is negative whereas $\nabla\cdot\mathbf{J}_i$ is positive. This implies that part of the inertial current $\mathbf{J}_i$ is converted to upward FAC (negative $J_{\parallel}$). However, it is uncertain if all the substorm-associated FAC is connected to the inertial current. At off-equator, $\nabla\cdot\mathbf{J}_{\parallel}$ is positive, indicating that the upward FAC is degraded. Most of the FACs are connected to the diamagnetic current $\mathbf{J}_d$ at high latitudes. Figure 4e shows the rate of change in the FAC, $\partial J_{\parallel}/\partial t$, which is obtained on the basis of Ampère and Faraday laws. The black solid line indicates $-(\nabla\times\nabla\times\mathbf{E})_{\parallel}/\mu_0$ $(=\partial J_{\parallel}/\partial t)$, which is negative at $D \sim 0.3$–2.6 R_E and $D \sim 4.5$–5.2 R_E. The contributions from $-\nabla_{\parallel}(\nabla\cdot\mathbf{E})/\mu_0$ (red line) and $(\nabla^2\mathbf{E})_{\parallel}/\mu_0$ (blue line) are equally important. The sum of the two terms is not always equal to $-(\nabla\times\nabla\times\mathbf{E})_{\parallel}/\mu_0$ because of numerical errors. We calculated these terms by the central difference method in Cartesian coordinates with a finite distance h. The tendency is unchanged for different h. Therefore, we cannot determine quantitatively the contributions from these terms definitively, but the conclusion remains that these two terms, $-\nabla_{\parallel}(\nabla\cdot\mathbf{E})/\mu_0$ and $(\nabla^2\mathbf{E})_{\parallel}/\mu_0$, are equally important. Figure 4f shows $\mathbf{J}\cdot\mathbf{E}$, $\mathbf{V}\cdot\mathbf{F}_t$ and $\mathbf{V}\cdot\mathbf{F}_m$. Obviously, $\mathbf{V}\cdot\mathbf{F}_t$ is negative near the equatorial plane at $D \sim 4.0$–5.4 R_E, implying that the Alfvén waves are excited there. Note that $\mathbf{J}\cdot\mathbf{E}$ is negative at off-equator at $D \sim 0.7$–4.7 R_E. The negative $\mathbf{V}\cdot\mathbf{F}_t$ region does not coincide with the negative $\mathbf{J}\cdot\mathbf{E}$ region. By considering the 3 aspects, we speculate that the substorm-associated upward FAC is generated at $D \sim 4.7$–5.2 R_E, which is shaded by the light blue color. We call this region near-Earth FAC dynamo. The near-Earth FAC has the following characteristics. First, $\nabla\cdot\mathbf{J}_{\parallel} < 0$ for upward FAC $(J_{\parallel} < 0)$ when the FAC is converted from the field-perpendicular current. Secondly, $-(\nabla\times\nabla\times\mathbf{E})_{\parallel}/\mu_0 (=\partial J_{\parallel}/\partial t) < 0$ for upward FAC. That is, the FAC is required by Ampère and Faraday laws. Thirdly, $\mathbf{V}\cdot\mathbf{F}_t < 0$. That is, the Alfvén waves are excited.

Next, we investigated the origin of the plasma that is involved in the excitation of the Alfvén waves (i.e., $\mathbf{V}\cdot\mathbf{F}_t < 0$) by tracing a stream line backward in time from an arbitrary selected position in the near-Earth FAC dynamo at $(-7.2, 1.2, 0.4)$ R_E at $t = 177.49$ min. We refer this point Q, which is indicated in Figure 2. The stream line is an integral curve of velocity $\mathbf{V}$ with respect to time. The quantities taken along the stream line are shown in Figure 5. The plasma element is found to originate in the tail lobe region that is characterized by low speed and low plasma pressure. The plasma element travels from the tail lobe region to the near-Earth FAC dynamo by way of the following characteristic regions. (a) The plasma element moves toward the equatorial plane (plasma sheet). (b) The plasma element is accelerated earthward (in the x-direction) by the Lorentz force as shown in Figure 5d. The power density shown in Figure 5f indicates that the magnetic energy is converted to the kinetic energy and the internal energy (i.e., $-\mathbf{V}\cdot(\mathbf{J}\times\mathbf{B}) < 0$, $\mathbf{V}\cdot(\mathbf{J}\times\mathbf{B}-\nabla P) > 0$ and $\mathbf{V}\cdot\nabla P > 0$), which is consistent with Birn and Hesse (2005). (c) As the plasma element approaches $x \sim -9$ R_E, it is decelerated by the pressure gradient force, followed by the Lorentz force (Figure 5d). The kinetic energy is converted to the internal energy, followed by the magnetic energy (Figure 5f) (i.e., $\mathbf{V}\cdot(\mathbf{J}\times\mathbf{B}-\nabla P) < 0$, $\mathbf{V}\cdot\nabla P > 0$ and $-\mathbf{V}\cdot(\mathbf{J}\times\mathbf{B}) > 0$). The increase in the internal energy results in the increase in the plasma pressure (Figure 5h). (d) The plasma element is gradually deflected to the y-direction (duskward) by the Lorentz force and the pressure gradient force (Figure 5e), and arrives at the near-Earth FAC dynamo. The magnetic energy and the internal energy are converted to the kinetic energy (Figure 5g). Part of the kinetic energy is used to excite the Alfvén waves (i.e., $\mathbf{V}\cdot\mathbf{F}_t < 0$) as shown in Figure 4f.

Figure 6 presents a schematic drawing of the potential process for the generation of the FACs that appear abruptly around the beginning of the substorm expansion phase. The near-Earth reconnection results in the earthward fast flow of plasma as indicated by the yellow arrow. The earthward flow is decelerated, and is diverted to the dawn and dusk directions. The substorm-associated FACs are generated in near-Earth region (near-Earth FAC dynamo)

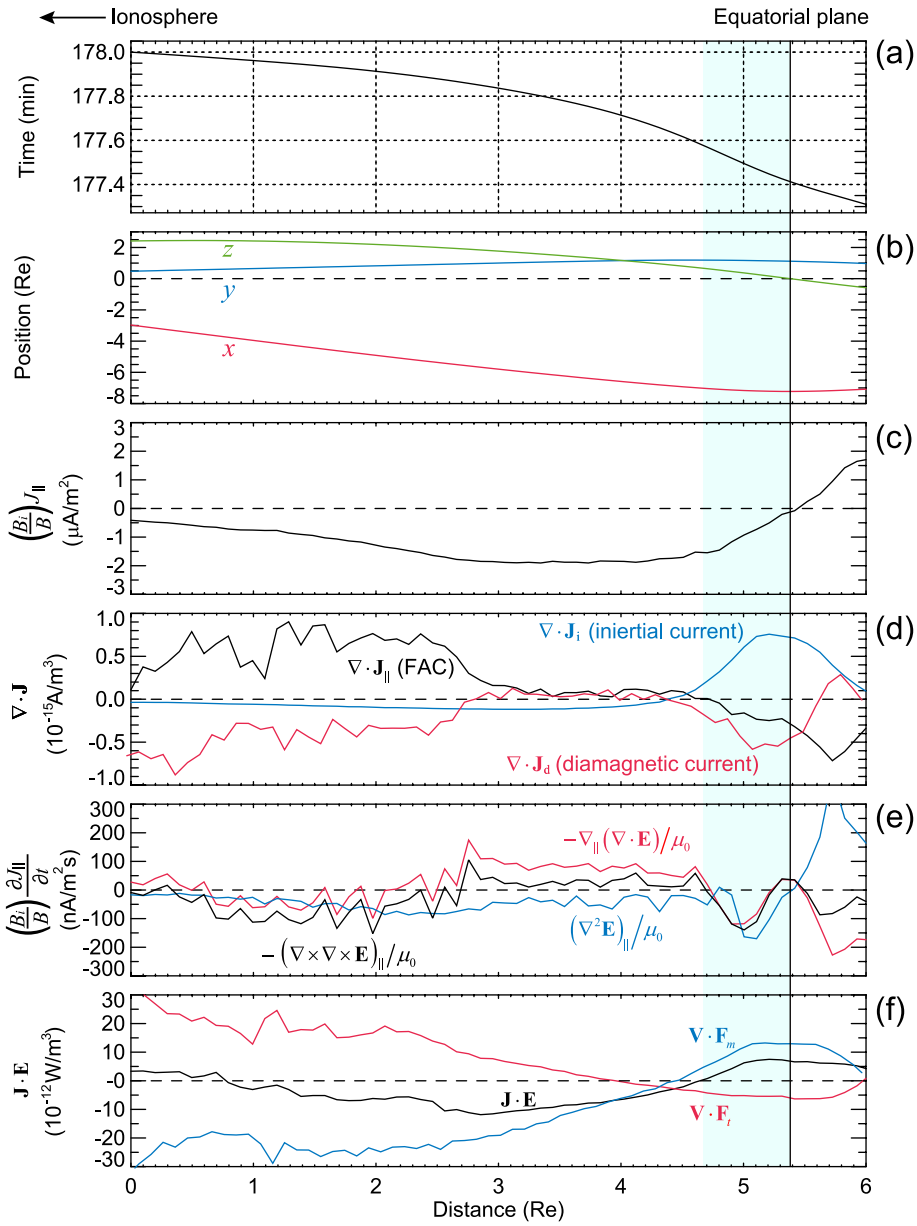

Figure 4. Quantities taken along the trajectory of the packet of the Alfvén wave arriving at the point *P*′ (whose footprint is point *P*, i.e., 66.6 MLAT and 23.4 MLT) at $t = 178.00$ min. (a) Time t, (b) position, (c) normalized FAC $(B_i/B)J_{\parallel}$ (negative upward FAC), (d) $\nabla\cdot\mathbf{J}_{\parallel}$, $\nabla\cdot\mathbf{J}_d$, and $\nabla\cdot\mathbf{J}_i$, where $\mathbf{J}_{\parallel}$, $\mathbf{J}_d$ and $\mathbf{J}_i$ are the FAC, the diamagnetic current and the inertial current, respectively, (e) the rate of change in the FAC, $\partial J_{\parallel}/\partial t$, (f) $\mathbf{J}\cdot\mathbf{E}$ (black), $\mathbf{V}\cdot\mathbf{F}_t$ (red) and $\mathbf{V}\cdot\mathbf{F}_m$ (blue), where $\mathbf{F}_t$ and $\mathbf{F}_m$, are the magnetic tension force and the magnetic pressure force, respectively are shown as a function of arc length (distance) from the point *P*′ along the trajectory. The vertical line indicates the equatorial plane. The bluish area indicates the near-Earth FAC dynamo in which the substorm-associated Region 1-sense FAC is generated.

in which the following three processes occur simultaneously. (a) The azimuthally moving plasma performs negative work against the magnetic tension force, that is, $\mathbf{V}\cdot\mathbf{F}_t < 0$ where $\mathbf{F}_t$ is the magnetic tension force. The Alfvén waves are excited. (b) The FACs are generated, that is, $\partial J_{\parallel}/\partial t > 0$ on the dawnside, and $\partial J_{\parallel}/\partial t < 0$ on the duskside (positive downward in the Northern Hemisphere) on the basis of Ampère's and Faraday's laws. (c) The field-perpendicular current is converted to the FACs, that is, $\nabla\cdot\mathbf{J}_{\parallel} > 0$ for the downward FAC ($\partial J_{\parallel}/\partial t > 0$), and $\nabla\cdot\mathbf{J}_{\parallel} < 0$ for the upward FAC ($\partial J_{\parallel}/\partial t < 0$) on the basis of current continuity. The Alfvén waves propagate along the magnetic field in the rest frame of moving medium together with the FACs. When it arrives at the ionosphere, the westward auroral electrojet starts increasing abruptly, and the substorm expansion phase begins.

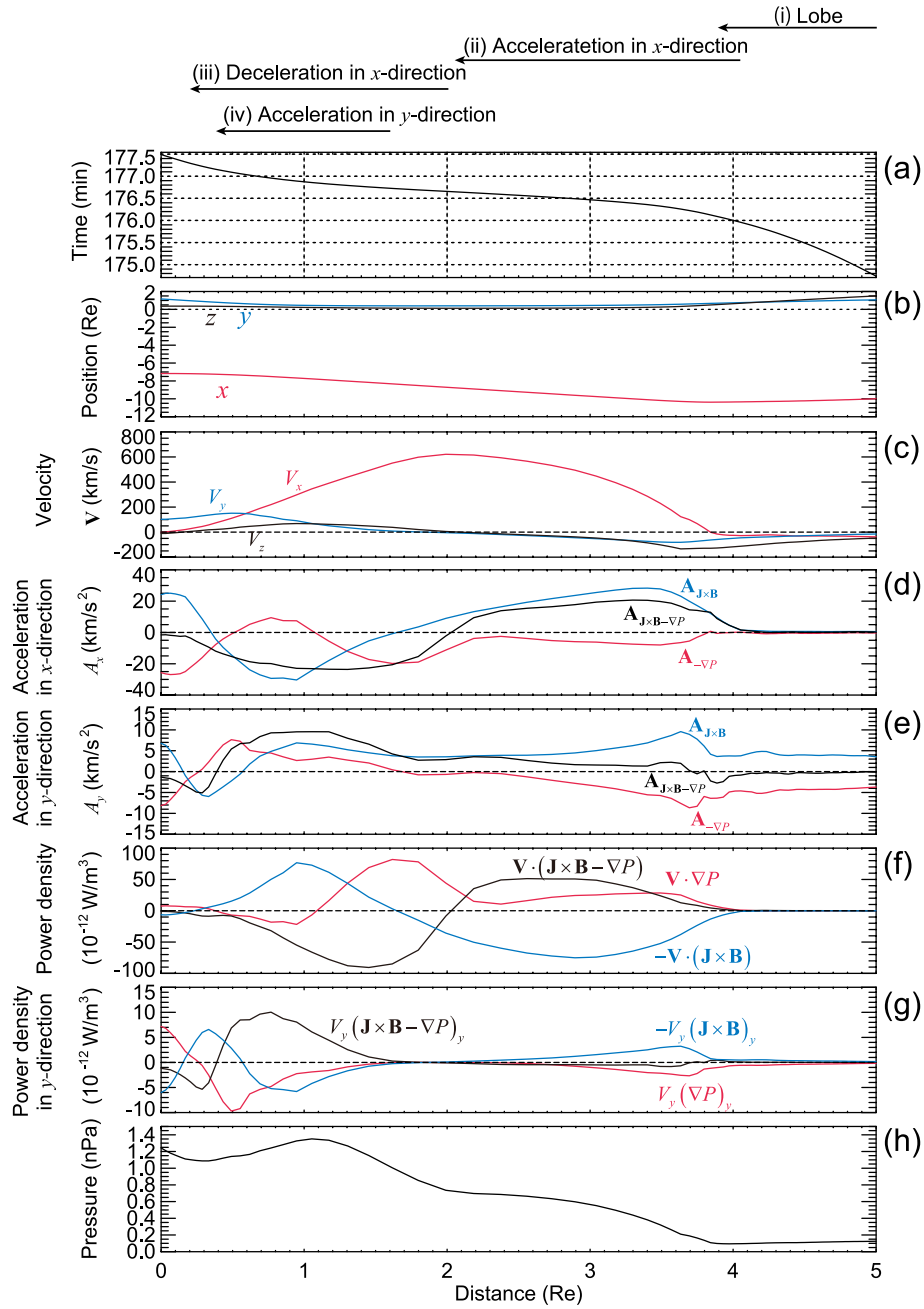

Figure 5. Quantities taken along the stream line (line integral of velocity of plasma with respect to time) that arrives at the point Q (−7.2, 1.2, 0.4) R_E at t = 177.49 min. The point Q is located in the near-Earth FAC dynamo, and indicated in Figure 2. From top to bottom, (a) time t, (b) position, (c) velocity $\mathbf{V}$, (d) x-component of the acceleration, (e) y-component of the acceleration, (f) power density, (g) power density derived from the values in the y-direction, and (h) plasma pressure P are shown as a function of arc length (distance) from the point Q (in the near-Earth FAC dynamo) along the trajectory. In (d) and (e), the black, the red, and the blue lines indicate acceleration due to the inertial force, the Lorentz force, and the plasma pressure force, respectively. In (f) and (g), the red, the blue, and the green lines indicate the power densities of $\mathbf{V}\cdot\nabla P$, $\mathbf{V}\cdot(\mathbf{J}\times\mathbf{B}-\nabla P)$, and $-\mathbf{V}\cdot(\mathbf{J}\times\mathbf{B})$, respectively. When these values are positive, the internal energy, the kinetic energy, and the magnetic energy increase, respectively.

5. Discussion and Conclusion

By using the global MHD simulation, we investigated the origin and the generation process of the field-aligned currents (FACs) that abruptly appear around the beginning of the substorm expansion phase. In the simulation,

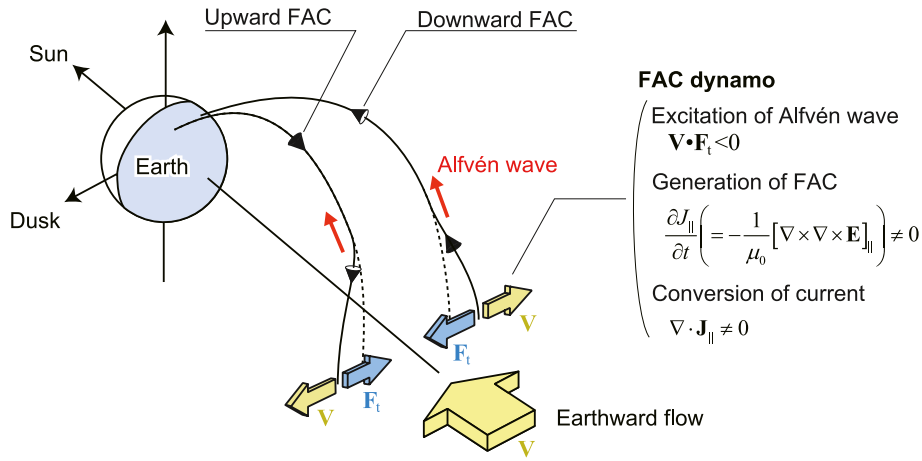

Figure 6. Schematic illustration showing the possible generation mechanism of the substorm-associated FACs. The black lines indicate the instantaneous magnetic field lines. The yellow arrows indicate the flow of plasma. The blue arrows indicate the direction of the magnetic tension force $\mathbf{F}_t$. The substorm-associated FAC is generated in the near-Earth FAC dynamo in which the plasma performs negative work against the magnetic tension force ($\mathbf{V}\cdot\mathbf{F}_t < 0$), the rate of change in the FAC ($J_\parallel$) is nonzero and the field-perpendicular current is converted to the FACs. The earthward fast flow is split into the dawn and dusk flows, which pull the magnetic field lines. See text for detailed explanation.

the FACs are generated near the equatorial plane in the near-Earth region, in which (a) plasma performs negative work against the magnetic tension force (Figure 4f), (b) the rate of change in the FACs is nonzero on the basis of Ampère's and Faraday's laws (Figure 4e), and (c) the field-perpendicular current is converted to FAC (Figure 4d). We call it near-Earth FAC dynamo.

It has been suggested from the MHD simulations that just before the expansion onset, the negative $\mathbf{J}\cdot\mathbf{E}$ region appears in the near-Earth region, which is referred to as near-Earth dynamo (Birn et al., 2004; Ebihara and Tanaka, 2015a, 2015b; Tanaka et al., 2010, 2017). Ebihara and Tanaka (2015b) showed no clear one-to-one correspondence between the region where $\mathbf{J}\cdot\mathbf{E} < 0$ and the generation of the FACs. They suggested that the rate of change in the magnetic energy $\partial(B^2/2\mu_0)/\partial t$ could also have participated in the generation of FACs. However, it is not straightforward that the change in the magnetic energy is directly associated with the generation of the FACs. This issue is reasonably resolved by considering $\mathbf{V}\cdot\mathbf{F}_t$, instead of considering $\mathbf{J}\cdot\mathbf{E}$. As demonstrated in Figure 4f, the near-Earth FAC dynamo (where $\mathbf{V}\cdot\mathbf{F}_t < 0$) does not always coincide with the near-Earth dynamo (where $\mathbf{J}\cdot\mathbf{E} < 0$) because of the substantial contribution from $\mathbf{V}\cdot\mathbf{F}_m$. When $\mathbf{V}\cdot\mathbf{F}_m$ is negative, the magnetic field is supposed to be compressed, but not be immediately related to the generation of the Alfvén waves.

We traced the packet from the point P (onset point) at $t = 178.0$ min backward in time. The magnetic field line extending from the point P passes through the equatorial plane at ~23.2 MLT when we used the instantaneous magnetic field at $t = 178.0$ min. The packet passes through the equatorial plane at ~23.4 MLT. This implies that the packet was deflected westward by ~0.2 hr in MLT in the course of the travel from the equatorial plane to the Earth. The deflection is small, and may be negligible. The Alfvén travel time from the equatorial plane to the ionosphere is only ~0.6 min, but may be nonnegligible. The quantities taken along the instantaneous magnetic field line (shown in Figure 8 of Ebihara and Tanaka (2015b)) are fully different from those taken along the trajectory of packet (shown in Figure 4 of this paper). Considering the travel time of the Alfvén wave is necessary to understand the generation processes of the FACs properly.

With the Ohm's law, $\mathbf{E} = -\mathbf{V}\times\mathbf{B}$, $\nabla\cdot\mathbf{E} = \nabla\cdot(-\mathbf{V}\times\mathbf{B}) = -\mathbf{B}\cdot(\nabla\times\mathbf{V}) + \mathbf{V}\cdot(\nabla\times\mathbf{B})$. The term $(\nabla\times\mathbf{V})_\parallel$ is often referred to as the flow shear, or vorticity, and is used to describe the generation of the substorm-associated FACs (Keiling et al., 2009). The first term ($-\mathbf{B}\cdot(\nabla\times\mathbf{V})$) is negative on the duskside because the earthward flow deflects toward dusk. However, in the simulation, the second term ($\mathbf{V}\cdot(\nabla\times\mathbf{B})$) is positive near the equatorial plane (not shown). A sum of these two terms yields positive $\nabla\cdot\mathbf{E}$ near the equatorial plane. This is opposite to that simply expected from $(\nabla\times\mathbf{V})_\parallel$. This implies that the second term ($\mathbf{V}\cdot(\nabla\times\mathbf{B})$) is non-negligible, and that the care must be needed to evaluate $\nabla\cdot\mathbf{E}$ from $\mathbf{V}$ (or vorticity). In addition, the contribution from $(\nabla^2\mathbf{E})_\parallel/\mu_0$ is also important as shown in Figure 4e. Probably, the FAC is no longer a simple projection of $\nabla\cdot\mathbf{E}$, nor $(\nabla\times\mathbf{V})_\parallel$ in the equatorial plane.

According to the global MHD simulation, the Region 1 FAC is generated in the flank FAC dynamo (Ebihara & Tanaka, 2022), and the substorm-associated FAC is generated in the near-Earth FAC dynamo (this study). These FAC dynamo regions are separated in space, but the processes are similar. First, the plasma pulls the magnetic field line, that is, $\mathbf{V}\cdot\mathbf{F}_t$ is negative to excite the Alfvén waves. Flow of solar wind-originated plasma (and magnetosphere-originated plasma) is involved in the flank FAC dynamo, whereas azimuthally deflected flow coming from the near-Earth reconnection site is involved in the near-Earth FAC dynamo. Secondly, the negative $\mathbf{V}\cdot\mathbf{F}_t$ region does not always coincide with the negative $\mathbf{J}\cdot\mathbf{E}$ region. Thirdly, the contributions from $-\nabla_{\parallel}(\nabla\cdot\mathbf{E})/\mu_0$ and $(\nabla^2\mathbf{E})_{\parallel}/\mu_0$ are equally important for the generation of FACs. When the flank FAC dynamo starts working, the growth phase begins. When the near-Earth FAC dynamo starts working, the expansion phase begins. It is suggested that the FAC dynamo regions govern the transition of the substorm phases, and that the evolution of the substorm can also be described in terms of the development of the FAC dynamo regions.

We suggest the following processes that may occur around the substorm expansion phase. On the basis of the results shown above, we updated the items 4 and 5.

1. When the magnetic reconnection takes place in the near-Earth plasma sheet, earthward fast flow appears (Angelopoulos et al., 2008; Baker et al., 2002; Hones et al., 1973; Ieda et al., 2008; Machida et al., 2009; Miyashita et al., 2009; Nishida & Nagayama, 1973; Runov et al., 2008; Sergeev et al., 1995; Yao et al., 2012). The magnetic energy (originating in the tail lobe region) splits into the internal energy and the kinetic energy (Birn et al., 2011; Birn & Hesse, 2005).
2. As the earthward fast flow is decelerated (Shiokawa et al., 1997), the plasma pressure increases due to compression (Ebihara & Tanaka, 2015b; Tanaka et al., 2010, 2016). The increase in the plasma pressure is observed in the near-Earth tail region (Yao et al., 2015a, 2015b). In the course of the deceleration, the kinetic energy is converted to the internal energy and the magnetic energy in the near-Earth region.
3. The plasma is accelerated eastward and westward by the plasma pressure gradient force and the Lorentz force. The internal energy and the magnetic energy are converted to the kinetic energy.
4. Near-Earth FAC dynamo starts working. The plasma moving in the east and west directions performs negative work against the magnetic tension force, that is, $\mathbf{V}\cdot\mathbf{F}_t$ is negative. The kinetic energy is converted to the magnetic energy that is used to excite the Alfvén waves. FACs are generated from the requirement of Ampère's and Faraday's laws. Part of the inertial current is converted to the FAC in the near-Earth FAC dynamo.
5. The Alfvén waves travel along the magnetic field in the rest frame of moving plasma together with FAC. When the upward FAC approaches the ionosphere along with the Alfvén waves, a number of electrons will be accelerated downward, resulting in bright discrete auroras (Korth et al., 2014).

Of course, kinetic processes as well as non-MHD processes may also participate in the evolution of substorms, such as instabilities in the plasma sheet, electron precipitation, and 3-dimensional closure in the ionosphere. These issues remain, and will be solved in future.

Data Availability Statement

The simulation data used in this study are available at http://doi.org/10.5281/zenodo.7066189.

Acknowledgments
The computer simulation was performed on the KDK computer system at the Research Institute for Sustainable Humanosphere (RISH), Kyoto University. This study was supported by JSPS KAKENHI Grant 20H01960 and 20H01957.

References

Ahn, B. H., Akasofu, S. I., & Kamide, Y. (1983). The Joule heat production rate and the particle energy injection rate as a function of the geomagnetic indices AE and AL. *Journal of Geophysical Research*, *88*(A8), 6275. https://doi.org/10.1029/JA088iA08p06275

Akasofu, S. I. (1964). The development of the auroral substorm. *Planetary and Space Science*, *12*(4), 273–282. https://doi.org/10.1016/0032-0633(64)90151-5

Akasofu, S.-I. (2013). Where is the magnetic energy for the expansion phase of auroral substorms accumulated? *Journal of Geophysical Research: Space Physics*, *118*(11), 7219–7225. https://doi.org/10.1002/2013JA019042

Anderson, B. J., Korth, H., Waters, C. L., Green, D. L., Merkin, V. G., Barnes, R. J., & Dyrud, L. P. (2014). Development of large-scale Birkeland currents determined from the active magnetosphere and planetary electrodynamics Response Experiment. *Geophysical Research Letters*, *41*(9), 3017–3025. https://doi.org/10.1002/2014GL059941

Angelopoulos, V., Coroniti, F. V., Kennel, C. F., Kivelson, M. G., Walker, R. J., Russell, C. T., et al. (1996). Multipoint analysis of a bursty bulk flow event on April 11, 1985. *Journal of Geophysical Research*, *101*(A3), 4967–4989. https://doi.org/10.1029/95ja02722

Angelopoulos, V., McFadden, J. P., Larson, D., Carlson, C. W., Mende, S. B., Frey, H., et al. (2008). Tail reconnection triggering substorm onset. *Science*, *321*(5891), 931–935. https://doi.org/10.1126/science.1160495

Baker, D. N., Peterson, W. K., Eriksson, S., Li, X., Blake, J. B., Burch, J. L., et al. (2002). Timing of magnetic reconnection initiation during a global magnetospheric substorm onset. *Geophysical Research Letters*, *29*(24), 4341–4344. https://doi.org/10.1029/2002gl015539

Baker, D. N., Pulkkinen, T. I., McPherron, R. L., Craven, J. D., Frank, L. A., Elphinstone, R. D., et al. (1993). CDAW 9 analysis of magnetospheric events on May 3, 1986: Event C. *Journal of Geophysical Research*, *98*(A3), 3815–3834. https://doi.org/10.1029/92JA02475

Birn, J., & Hesse, M. (1991). The substorm current wedge and field-aligned currents in MHD simulations of magnetotail reconnection. *Journal of Geophysical Research*, *96*(A2), 1611–1618. https://doi.org/10.1029/90JA01762

Birn, J., & Hesse, M. (1996). Details of current disruption and diversion in simulations of magnetotail dynamics. *Journal of Geophysical Research*, *101*(A7), 15345–15358. https://doi.org/10.1029/96JA00887

Birn, J., & Hesse, M. (2005). Energy release and conversion by reconnection in the magnetotail. *Annales Geophysicae*, *23*(10), 3365–3373. https://doi.org/10.5194/angeo-23-3365-2005

Birn, J., & Hesse, M. (2013). The substorm current wedge in MHD simulations. *Journal of Geophysical Research: Space Physics*, *118*(6), 3364–3376. https://doi.org/10.1002/jgra.50187

Birn, J., Hesse, M., Haerendel, G., Baumjohann, W., & Shiokawa, K. (1999). Flow braking and the substorm current wedge. *Journal of Geophysical Research*, *104*(A9), 19895–19903. https://doi.org/10.1029/1999ja900173

Birn, J., Hesse, M., & Zenitani, S. (2011). Reconnection in compressible plasmas: Extended conversion region. *Physics of Plasmas*, *18*(11), 111202. https://doi.org/10.1063/1.3626836

Birn, J., Raeder, J., Wang, Y. L., Wolf, R. A., & Hesse, M. (2004). On the propagation of bubbles in the geomagnetic tail. *Annales Geophysicae*, *22*(5), 1773–1786. https://doi.org/10.5194/angeo-22-1773-2004

Boström, R. (1964). A model of the auroral electrojets. *Journal of Geophysical Research*, *69*(23), 4983–4999. https://doi.org/10.1029/JZ069i023p04983

Chen, C. X., & Wolf, R. A. (1993). Interpretation of high-speed flows in the plasma sheet. *Journal of Geophysical Research*, *98*(A12), 21409–21419. https://doi.org/10.1029/93JA02080

Cheng, C. Z., & Lui, A. T. Y. (1998). Kinetic ballooning instability for substorm onset and current disruption observed by AMPTE/CCE. *Geophysical Research Letters*, *25*(21), 4091–4094. https://doi.org/10.1029/1998GL900093

Connors, M., McPherron, R. L., Anderson, B. J., Korth, H., Russell, C. T., & Chu, X. (2014). Electric currents of a substorm current wedge on 24 February 2010. *Geophysical Research Letters*, *41*(13), 4449–4455. https://doi.org/10.1002/2014GL060604

Coxon, J. C., Milan, S. E., Clausen, L. B. N., Anderson, B. J., & Korth, H. (2014a). The magnitudes of the regions 1 and 2 Birkeland currents observed by AMPERE and their role in solar wind-magnetosphere-ionosphere coupling. *Journal of Geophysical Research: Space Physics*, *119*(12), 9804–9815. https://doi.org/10.1002/2014JA020138

Coxon, J. C., Milan, S. E., Clausen, L. B. N., Anderson, B. J., & Korth, H. (2014b). A superposed epoch analysis of the regions 1 and 2 Birkeland currents observed by AMPERE during substorms. *Journal of Geophysical Research: Space Physics*, *119*(12), 9834–9846. https://doi.org/10.1002/2014ja020500

Coxon, J. C., Rae, I. J., Forsyth, C., Jackman, C. M., Fear, R. C., & Anderson, B. J. (2017). Birkeland currents during substorms: Statistical evidence for intensification of Regions 1 and 2 currents after onset and a localized signature of auroral dimming. *Journal of Geophysical Research: Space Physics*, *122*(6), 6455–6468. https://doi.org/10.1002/2017JA023967

Cravens, T. E. (1997). *Physics of solar system plasmas*. Cambridge University Press. https://doi.org/10.1017/CBO9780511529467

Crooker, N. U., & McPherron, R. L. (1972). On the distinction between the auroral electrojet and partial ring current systems. *Journal of Geophysical Research*, *77*(34), 6886–6889. https://doi.org/10.1029/JA077i034p06886

Cummings, W. D., Barfield, J. N., & Coleman, P. J. (1968). Magnetospheric substorms observed at the synchronous orbit. *Journal of Geophysical Research*, *73*(21), 6687–6698. https://doi.org/10.1029/JA073i021p06687

Davis, T. N., & Sugiura, M. (1966). Auroral electrojet activity index AE and its universal time variations. *Journal of Geophysical Research*, *71*(3), 785–801. https://doi.org/10.1029/JZ071i003p00785

Donovan, E. F., Mende, S., Jackel, B., Syrjäsuo, M., Meurant, M., Voronkov, I., et al. (2006). The azimuthal evolution of the substorm expansive phase onset aurora. *Proceedings of ICS-8*, 55–60.

Ebihara, Y., & Tanaka, T. (2015a). Substorm simulation: Formation of westward traveling surge. *Journal of Geophysical Research: Space Physics*, *120*(12), 10466–10484. https://doi.org/10.1002/2015JA021697

Ebihara, Y., & Tanaka, T. (2015b). Substorm simulation: Insight into the mechanisms of initial brightening. *Journal of Geophysical Research A: Space Physics*, *120*(9), 7270–7288. https://doi.org/10.1002/2015JA021516

Ebihara, Y., & Tanaka, T. (2022). Where is region 1 field-aligned current generated? *Journal of Geophysical Research: Space Physics*, *127*(3). https://doi.org/10.1029/2021ja029991

Ebihara, Y., Tanaka, T., & Kikuchi, T. (2014). Counter equatorial electrojet and overshielding after substorm onset: Global MHD simulation study. *Journal of Geophysical Research: Space Physics*, *119*(9), 7281–7296. https://doi.org/10.1002/2014JA020065

Fairfield, D. H., Mukai, T., Lui, A. T. Y., Cattell, C. A., Reeves, G. D., Nagai, T., et al. (1998). Geotail observations of substorm onset in the inner magnetotail. *Journal of Geophysical Research*, *103*(A1), 103–117. https://doi.org/10.1029/97ja02043

Gjerloev, J. W., & Hoffman, R. A. (2014). The large-scale current system during auroral substorms. *Journal of Geophysical Research: Space Physics*, *119*(6), 4591–4606. https://doi.org/10.1002/2013JA019176

Haerendel, G. (1992). *Disruption, ballooning or auroral avalanche-on the cause of substorms* (pp. 417–420). ESA Publications Division.

Hamrin, M., Marghitu, O., Norqvist, P., Buchert, S., André, M., Klecker, B., et al. (2011). Energy conversion regions as observed by cluster in the plasma sheet. *Journal of Geophysical Research*, *116*(A1), A00K08. https://doi.org/10.1029/2010JA016383

Hamrin, M., Marghitu, O., Rönnmark, K., Klecker, B., André, M., Buchert, S., et al. (2006). Observations of concentrated generator regions in the nightside magnetosphere by Cluster/FAST conjunctions. *Annales Geophysicae*, *24*(2), 637–649. https://doi.org/10.5194/angeo-24-637-2006

Hasegawa, A., & Sato, T. (1979). Generation of field aligned current during substorm. In S. I. Akasofu (Ed.), *Dynamics of the magnetosphere. Astrophysics and space science library* (pp. 529–542). Springer. https://doi.org/10.1007/978-94-009-9519-2_28

Hesse, M., & Birn, J. (1991). On dipolarization and its relation to the substorm current wedge. *Journal of Geophysical Research*, *96*(A11), 19417. https://doi.org/10.1029/91JA01953

Hones, E. W. (1979). Transient phenomena in the magnetotail and their relation to substorms. *Space Science Reviews*, *23*(3), 393–410. https://doi.org/10.1007/BF00172247

Hones, E. W., Asbridge, J. R., Bame, S. J., & Singer, S. (1973). Substorm variations of the magnetotail plasma sheet from X SM ≈ −6 R E to X SM ≈ −60 R E. *Journal of Geophysical Research*, *78*(1), 109–132. https://doi.org/10.1029/JA078i001p00109

Hughes, T. J., & Rostoker, G. (1979). A comprehensive model current system for high-latitude magnetic activity - I. The steady state system. *Geophysical Journal International*, *58*(3), 525–569. https://doi.org/10.1111/j.1365-246X.1979.tb04793.x

Ieda, A., Fairfield, D. H., Slavin, J. A., Liou, K., Meng, C.-I., Machida, S., et al. (2008). Longitudinal association between magnetotail reconnection and auroral breakup based on Geotail and Polar observations. *Journal of Geophysical Research*, *113*(8), A08207. https://doi.org/10.1029/2008JA013127

Iijima, T., & Potemra, T. A. (1976). The amplitude distribution of field-aligned currents at northern high latitudes observed by Triad. *Journal of Geophysical Research*, *81*(13), 2165–2174. https://doi.org/10.1029/JA081i013p02165

Iijima, T., & Potemra, T. A. (1978). Large-scale characteristics of field-aligned currents associated with substorms. *Journal of Geophysical Research*, *83*(A2), 599. https://doi.org/10.1029/JA083iA02p00599

Itonaga, M., Yoshikawa, A., & Fujita, S. (2000). A wave equation describing the generation of field-aligned current in the magnetosphere. *Earth Planets and Space*, *52*(7), 503–507. https://doi.org/10.1186/BF03351654

Kamide, Y., & Akasofu, S. I. (1976). The location of the field-aligned currents with respect to discrete auroral arcs. *Journal of Geophysical Research*, *81*(22), 3999–4003. https://doi.org/10.1029/JA081i022p03999

Kamide, Y., & Baumjohann, W. (1985). Estimation of electric fields and currents from international magnetospheric study magnetometer data for the CDAW 6 intervals: Implications for substorm dynamics. *Journal of Geophysical Research*, *90*(A2), 1305. https://doi.org/10.1029/JA090iA02p01305

Kamide, Y., & Brekke, A. (1975). Auroral electrojet current density deduced from the Chatanika Radar and from the Alaska Meridian Chain of magnetic observatories. *Journal of Geophysical Research*, *80*(4), 587–594. https://doi.org/10.1029/JA080i004p00587

Kamide, Y., Craven, J. D., Frank, L. A., Ahn, B. h., & Akasofu, S. I. (1986). Modeling substorm current systems using conductivity distributions inferred from DE auroral images. *Journal of Geophysical Research*, *91*(A10), 11235. https://doi.org/10.1029/JA091iA10p11235

Kamide, Y., & Fukushima, N. (1972). Positive geomagnetic bays in evening high-latitudes and their possible connection with partial ring current. *Report of Ionosphere and Space Research in Japan*, *26*(1–2), 79–101.

Kamide, Y., Ishihara, Y., Killeen, T. L., Craven, J. D., Frank, L. A., & Heelis, R. A. (1989). Combining electric field and aurora observations from DE 1 and 2 with ground magnetometer records to estimate ionospheric electromagnetic quantities. *Journal of Geophysical Research*, *94*(A6), 6723–6738. https://doi.org/10.1029/JA094iA06p06723

Kamide, Y., Yasuhara, F., & Akasofu, S. I. (1976). A model current system for the magnetospheric substorm. *Planetary and Space Science*, *24*(3), 215–222. https://doi.org/10.1016/0032-0633(76)90018-0

Keiling, A., Angelopoulos, V., Runov, A., Weygand, J., Apatenkov, S. V., Mende, S., et al. (2009). Substorm current wedge driven by plasma flow vortices: THEMIS observations. *Journal of Geophysical Research*, *114*(5), A00C22. https://doi.org/10.1029/2009JA014114

Kivelson, M. G. (2004). Moon–magnetosphere interactions: A tutorial. *Advances in Space Research*, *33*(11), 2061–2077. https://doi.org/10.1016/j.asr.2003.08.042

Korth, H., Zhang, Y., Anderson, B. J., Sotirelis, T., & Waters, C. L. (2014). Statistical relationship between large-scale upward field-aligned currents and electron precipitation. *Journal of Geophysical Research: Space Physics*, *119*(8), 6715–6731. https://doi.org/10.1002/2014ja019961

Lui, A. T. Y. (1991). A synthesis of magnetospheric substorm models. *Journal of Geophysical Research*, *96*(A2), 1849–1856. https://doi.org/10.1029/90ja02430

Lui, A. T. Y. (1996). Current disruption in the Earth's magnetosphere: Observations and models. *Journal of Geophysical Research*, *101*(A6), 13067–13088. https://doi.org/10.1029/96JA00079

Lui, A. T. Y. (2011). Reduction of the cross-tail current during near-Earth dipolarization with multisatellite observations. *Journal of Geophysical Research*, *116*(A12), A12239. https://doi.org/10.1029/2011JA017107

Lui, A. T. Y. (2015). Magnetospheric substorm onset by current disruption processes (pp. 163–176). https://doi.org/10.1002/9781118978719.ch12

Lui, A. T. Y., Chang, C. L., Mankofsky, A., Wong, H. K., & Winske, D. (1991). A cross-field current instability for substorm expansions. *Journal of Geophysical Research*, *96*(A7), 11389. https://doi.org/10.1029/91JA00892

Lui, A. T. Y., & Kamide, Y. (2003). A fresh perspective of the substorm current system and its dynamo. *Geophysical Research Letters*, *30*(18), 1958. https://doi.org/10.1029/2003GL017835

Lyons, L. R., Nishimura, Y., Shi, Y., Zou, S., Kim, H. J., Angelopoulos, V., et al. (2010). Substorm triggering by new plasma intrusion: Incoherent-scatter radar observations. *Journal of Geophysical Research*, *115*(A7), A07223. https://doi.org/10.1029/2009JA015168

Machida, S., Miyashita, Y., Ieda, A., Nosé, M., Nagata, D., Liou, K., et al. (2009). Statistical visualization of the Earth's magnetotail based on Geotail data and the implied substorm model. *Annales Geophysicae*, *27*(3), 1035–1046. https://doi.org/10.5194/angeo-27-1035-2009

Mallinckrodt, A. J., & Carlson, C. W. (1978). Relations between transverse electric fields and field-aligned currents. *Journal of Geophysical Research*, *83*(A4), 1426. https://doi.org/10.1029/JA083iA04p01426

Maltsev, Y. P., Lyatsky, W. B., & Lyatskaya, A. M. (1977). Currents over the auroral arc. *Planetary and Space Science*, 25(1), 53–57. https://doi.org/10.1016/0032-0633(77)90117-9

Marghitu, O., Hamrin, M., Klecker, B., Vaivads, A., McFadden, J., Buchert, S., et al. (2006). Experimental investigation of auroral generator regions with conjugate cluster and FAST data. *Annales Geophysicae*, *24*(2), 619–635. https://doi.org/10.5194/angeo-24-619-2006

McPherron, R. L., Russell, C. T., & Aubry, M. P. (1973). Satellite studies of magnetospheric substorms on August 15, 1968: 9. Phenomenological model for substorms. *Journal of Geophysical Research*, *78*(16), 3131–3149. https://doi.org/10.1029/ja078i016p03131

Meng, C. I., & Akasofu, S. I. (1969). A study of polar magnetic substorms: 2. Three-Dimensional current system. *Journal of Geophysical Research*, *74*(16), 4035–4053. https://doi.org/10.1029/JA074i016p04035

Miyashita, Y., Machida, S., Kamide, Y., Nagata, D., Liou, K., Fujimoto, M., et al. (2009). A state-of-the-art picture of substorm-associated evolution of the near-Earth magnetotail obtained from superposed epoch analysis. *Journal of Geophysical Research*, *114*(A1), A01211. https://doi.org/10.1029/2008JA013225

Motoba, T., Hosokawa, K., Kadokura, A., & Sato, N. (2012). Magnetic conjugacy of northern and southern auroral beads. *Geophysical Research Letters*, *39*(8). https://doi.org/10.1029/2012gl051599

Murphy, K. R., Mann, I. R., Rae, I. J., Waters, C. L., Frey, H. U., Kale, A., et al. (2013). The detailed spatial structure of field-aligned currents comprising the substorm current wedge. *Journal of Geophysical Research: Space Physics*, *118*(12), 7714–7727. https://doi.org/10.1002/2013JA018979

Nagai, T., & Shinohara, I. (2021). Dawn-dusk confinement of magnetic reconnection site in the near-Earth magnetotail and its implication for dipolarization and substorm current system. *Journal of Geophysical Research: Space Physics*, *126*(11). https://doi.org/10.1029/2021ja029691

Nagai, T., Singer, H. J., Mukai, T., Yamamoto, T., & Kokubun, S. (2000). Development of substorms in the near-Earth tail. *Advances in Space Research*, *25*(7–8), 1651–1662. https://doi.org/10.1016/s0273-1177(99)00680-8

Nakamura, R., Oguti, T., Yamamoto, T., & Kokubun, S. (1993). Equatorward and poleward expansion of the auroras during auroral substorms. *Journal of Geophysical Research*, *98*(A4), 5743–5759. https://doi.org/10.1029/92ja02230

Neubauer, F. M. (1980). Nonlinear standing Alfvén wave current system at Io: Theory. *Journal of Geophysical Research*, *85*(A3), 1171–1178. https://doi.org/10.1029/JA085iA03p01171

Newell, P. T., & Gjerloev, J. W. (2011). Evaluation of SuperMAG auroral electrojet indices as indicators of substorms and auroral power. *Journal of Geophysical Research*, *116*(12), A12211. https://doi.org/10.1029/2011JA016779

Nishida, A., & Nagayama, N. (1973). Synoptic survey for the neutral line in the magnetotail during the substorm expansion phase. *Journal of Geophysical Research*, *78*(19), 3782–3798. https://doi.org/10.1029/JA078i019p03782
Nishimura, Y., Lyons, L., Zou, S., Angelopoulos, V., & Mende, S. (2010). Substorm triggering by new plasma intrusion: THEMIS all-sky imager observations. *Journal of Geophysical Research*, *115*(A7), A07222. https://doi.org/10.1029/2009JA015166
Palmroth, M., Janhunen, P., Pulkkinen, T. I., Aksnes, A., Lu, G., Østgaard, N., et al. (2005). Assessment of ionospheric joule heating by GUMICS-4 MHD simulation, AMIE, and satellite-based statistics: Towards a synthesis. *Annales Geophysicae*, *23*(6), 2051–2068. https://doi.org/10.5194/angeo-23-2051-2005
Pritchett, P. L., & Coroniti, F. V. (2004). Three-dimensional collisionless magnetic reconnection in the presence of a guide field. *Journal of Geophysical Research*, *109*(A1), A01220. https://doi.org/10.1029/2003JA009999
Pu, Z. Y., Korth, A., & Kremser, G. (1992). Plasma and magnetic field parameters at substorm onsets derived from GEOS 2 observations. *Journal of Geophysical Research*, *97*(A12), 19341. https://doi.org/10.1029/92JA01732
Richmond, A. D., Kamide, Y., Akasofu, S.-I., Alcaydé, D., Blanc, M., De la Beaujardière, O., et al. (1990). Global measures of ionospheric electrodynamic activity inferred from combined incoherent scatter radar and ground magnetometer observations. *Journal of Geophysical Research*, *95*(A2), 1061. https://doi.org/10.1029/JA095iA02p01061
Rostoker, G., Armstrong, J. C., & Zmuda, A. J. (1975). Field-aligned current flow associated with intrusion of the substorm-intensified westward electrojet into the evening sector. *Journal of Geophysical Research*, *80*(25), 3571–3579. https://doi.org/10.1029/JA080i025p03571
Rostoker, G., & Boström, R. (1976). A mechanism for driving the gross Birkeland current configuration in the auroral oval. *Journal of Geophysical Research*, *81*(1), 235–244. https://doi.org/10.1029/JA081i001p00235
Roux, A., Perraut, S., Robert, P., Morane, A., Pedersen, A., Korth, A., et al. (1991). Plasma sheet instability related to the westward traveling surge. *Journal of Geophysical Research*, *96*(A10), 17697. https://doi.org/10.1029/91JA01106
Runov, A., Angelopoulos, V., Zhou, X.-Z., Voronkov, I. O., Kubyshkina, M. V., Nakamura, R., et al. (2008). Multipoint in situ and ground-based observations during auroral intensifications. *Journal of Geophysical Research*, *113*(A1), A00C07. https://doi.org/10.1029/2008ja013493
Sakaguchi, K., Shiokawa, K., Ieda, A., Nomura, R., Nakajima, A., Greffen, M., et al. (2009). Fine structures and dynamics in auroral initial brightening at substorm onsets. *Annales Geophysicae*, *27*(2), 623–630. https://doi.org/10.5194/angeo-27-623-2009
Sato, T., & Iijima, T. (1979). Primary sources of large-scale Birkeland currents. *Space Science Reviews*, *24*(3), 347–366. https://doi.org/10.1007/bf00212423
Sergeev, V. A., Angelopoulos, V., Mitchell, D. G., & Russell, C. T. (1995). In situ observations of magnetotail reconnection prior to the onset of a small substorm. *Journal of Geophysical Research*, *100*(A10), 19121. https://doi.org/10.1029/95ja01471
Shay, M. A., Drake, J. F., Eastwood, J. P., & Phan, T. D. (2011). Super-Alfvénic propagation of substorm reconnection signatures and Poynting flux. *Physical Review Letters*, *107*(6), 065001. https://doi.org/10.1103/PhysRevLett.107.065001
Shiokawa, K., Baumjohann, W., & Haerendel, G. (1997). Braking of high-speed flows in the near-Earth tail. *Geophysical Research Letters*, *24*(10), 1179–1182. https://doi.org/10.1029/97GL01062
Shiokawa, K., Haerendel, G., & Baumjohann, W. (1998). Azimuthal pressure gradient as driving force of substorm currents. *Geophysical Research Letters*, *25*(7), 959–962. https://doi.org/10.1029/98gl00540
Song, Y., & Lysak, R. L. (2001a). The physics in the auroral dynamo regions and auroral particle acceleration. *Physics and Chemistry of the Earth - Part C: Solar, Terrestrial & Planetary Science*, *26*(1–3), 33–42. https://doi.org/10.1016/S1464-1917(00)00087-8
Song, Y., & Lysak, R. L. (2001b). Towards a new paradigm: From a quasi-steady description to a dynamical description of the magnetosphere. *Space Science Reviews*, *95*(1–2), 273–292. https://doi.org/10.1023/A:1005288420253
Sorathia, K. A., Merkin, V. G., Panov, E. V., Zhang, B., Lyon, J. G., Garretson, J., et al. (2020). Ballooning-interchange instability in the near-Earth plasma sheet and auroral beads: Global magnetospheric modeling at the limit of the MHD approximation. *Geophysical Research Letters*, *47*(14), e2020GL088227. https://doi.org/10.1029/2020GL088227
Sun, W., Ahn, B. H., & Akasofu, S. I. (1985). The global joule heat production rate and the AE index. *Planetary and Space Science*, *33*(3), 279–281. https://doi.org/10.1016/0032-0633(85)90059-5
Takahashi, K., Zanetti, L. J., Lopez, R. E., McEntire, R. W., Potemra, T. A., & Yumoto, K. (1987). Disruption of the magnetotail current sheet observed by AMPTE/CCE. *Geophysical Research Letters*, *14*(10), 1019–1022. https://doi.org/10.1029/GL014i010p01019
Tanaka, T. (2015). Substorm auroral dynamics reproduced by advanced global magnetosphere–ionosphere (M–I) coupling simulation (pp. 177–190). https://doi.org/10.1002/9781118978719.ch13
Tanaka, T., Ebihara, Y., Watanabe, M., Den, M., Fujita, S., Kikuchi, T., et al. (2017). Global simulation study for the time sequence of events leading to the substorm onset. *Journal of Geophysical Research: Space Physics*, *122*(6), 6210–6239. https://doi.org/10.1002/2017JA024102
Tanaka, T., Ebihara, Y., Watanabe, M., Den, M., Fujita, S., Kikuchi, T., et al. (2021). Development of the substorm as a manifestation of convection transient. *Journal of Geophysical Research: Space Physics*, *126*(10). https://doi.org/10.1029/2020ja028942
Tanaka, T., Nakamizo, A., Yoshikawa, A., Fujita, S., Shinagawa, H., Shimazu, H., et al. (2010). Substorm convection and current system deduced from the global simulation. *Journal of Geophysical Research*, *115*(A5), A05220. https://doi.org/10.1029/2009JA014676
Tanaka, T., Watanabe, M., Den, M., Fujita, S., Ebihara, Y., Kikuchi, T., et al. (2016). Generation of field-aligned current (FAC) and convection through the formation of pressure regimes: Correction for the concept of Dungey's convection. *Journal of Geophysical Research: Space Physics*, *121*(9), 8695–8711. https://doi.org/10.1002/2016JA022822
Vasyliunas, V. (1970). Mathematical models of magnetospheric convection and its coupling to the ionosphere. In B. M. McCormac (Ed.), *Mathematical models of magnetospheric convection and its coupling to the ionosphere* (pp. 60–71). https://doi.org/10.1007/978-94-010-3284-1_6
Vasyliunas, V. M. (1984). Fundamentals of current description. *Magnetospheric Currents*, *28*, 63–66. https://doi.org/10.1029/GM028p0063
Walker, A. D. M. (2008). Ray tracing of magnetohydrodynamic waves in geospace. *URSI Radio Science Bulletin*, *2008*(325). https://doi.org/10.23919/URSIRSB.2008.7909583
Wright, A. N., & Southwood, D. J. (1987). Stationary Alfvénic structures. *Journal of Geophysical Research*, *92*(A2), 1167. https://doi.org/10.1029/JA092iA02p01167
Xing, X., Liang, J., Spanswick, E., Lyons, L., & Angelopoulos, V. (2013). Auroral wave structures and ballooning instabilities in the plasma sheet. *Journal of Geophysical Research: Space Physics*, *118*(10), 6319–6326. https://doi.org/10.1002/2013JA019068
Yang, J., Toffoletto, F. R., Wolf, R. A., Sazykin, S., Ontiveros, P. A., & Weygand, J. M. (2012). Large-scale current systems and ground magnetic disturbance during deep substorm injections. *Journal of Geophysical Research*, *117*(4), A04223. https://doi.org/10.1029/2011JA017415
Yao, Y., Ebihara, Y., & Tanaka, T. (2015a). Formation and evolution of high-plasma-pressure region in the near-Earth plasma sheet: Precursor and postcursor of substorm expansion onset. *Journal of Geophysical Research: Space Physics*, *120*(8), 6427–6435. https://doi.org/10.1002/2015JA021187
Yao, Y., Ebihara, Y., & Tanaka, T. (2015b). Sudden pressure enhancement and tailward retreat in the near-earth plasma sheet: THEMIS observation and MHD simulation. *Journal of Geophysical Research: Space Physics*, *120*(1), 201–211. https://doi.org/10.1002/2014JA020482

Yao, Z. H., Pu, Z. Y., Fu, S. Y., Angelopoulos, V., Kubyshkina, M., Xing, X., et al. (2012). Mechanism of substorm current wedge formation: THEMIS observations. *Geophysical Research Letters*, *39*(13), L13102. https://doi.org/10.1029/2012GL052055

Zenitani, S., & Nagai, T. (2016). Particle dynamics in the electron current layer in collisionless magnetic reconnection. *Physics of Plasmas*, *23*(10), 102102. https://doi.org/10.1063/1.4963008

Zmuda, A. J., & Armstrong, J. C. (1974). The diurnal flow pattern of field-aligned currents. *Journal of Geophysical Research*, *79*(31), 4611–4619. https://doi.org/10.1029/JA079i031p04611